Electronic Supplementary Information (ESI)

Table of Contents

Experimental Section

(○)-[Ru(S-*p*-^{t}BuC$_6$H$_4$)$_2$(CO)$_2$]$_8$, (○)-[Ru(S-*p*-^{i}PrC$_6$H$_4$)$_2$(CO)$_2$]$_6$, and (○)-{Cu[Ru(S-*p*-^{i}PrC$_6$H$_4$)$_2$(CO)$_2$]$_6$}PF$_6$ were prepared by the procedures reported previously.[1] ^{1}H NMR spectra were collected on a Bruker DRX-500 spectrometer. Electrospray ionization mass spectrometry (ESI-MS) analysis was performed on a Waters Micromass Q-Tof Premier quadrupole time-of-flight tandem mass spectrometer (Water Corporation, Milford, USA). Elemental analyses were conducted by the Institute of Chemistry, Chinese Academy of Sciences, Beijing.

Preparation of (○)- and (◇)-[Os(S-*p*-^{t}BuC$_6$H$_4$)$_2$(CO)$_2$]$_8$ mixture. A mixture of Os$_3$(CO)$_{12}$ (0.3 g, 0.33 mmol) and 4-*tert*-butyl-benzenethiol (2.0 mL, 12 mmol) was heated at 160 ℃ under argon for 12 h, and then cooled to room temperature. The reaction mixture changed colour from orange to yellow, with a yellow precipitate formed at the end of the reaction. The precipitate was collected by filtration, washed with diethyl ether, and dried. Yield: 23%. ^{1}H NMR (500 MHz, CDCl$_3$, 298 K): δ 8.44 (br s, 4H), 8.03 (m, 4H), 7.82 (d, *J* = 8.6 Hz, 8H), 7.67 (br s, 4H), 7.62 (m, 4H), 7.29 (d, *J* = 8.6 Hz, 4H), 7.23 (s, 16H), 7.11 (d, *J* = 8.7 Hz, 4H), 6.89 (m, 4H), 6.79 (d, *J* = 8.6 Hz, 8H), 6.45 (m, 4H), 5.73 (br, 4H), 1.59–1.05 (m, 216H) (the other signals were obscured or too broad to be observed). The ratio of the (○)-isomer to (◇)-isomer was estimated to be 0.5:1. Anal. Calcd for C$_{176}$H$_{208}$O$_{16}$Os$_8$S$_{16}$: C 45.81, H 4.54; found: C 45.70, H 4.82.

Preparation of (◇)-[Ru(S-*p*-^{t}BuC$_6$H$_4$)$_2$(CO)$_2$]$_8$. A mixture of Ru$_3$(CO)$_{12}$ (0.3 g, 0.45 mmol) and 4-*tert*-butyl-benzenethiol (2.0 mL, 12 mmol) was heated at 160 ℃ under argon for 12 h, and then cooled to room temperature. The reaction mixture changed colour from orange to yellow, with a yellow precipitate formed at the end of the reaction. The precipitate was collected by filtration, washed with diethyl ether, and dried. Yield: 34%. ^{1}H NMR (500 MHz, CDCl$_3$, 253 K): δ 8.69 (m, 4H), 8.11 (m, 4H), 7.83 (m, 4H), 7.67 (m, 4H), 7.33 (m, 4H), 7.24 (m, 8H), 7.11 (m, 8H), 6.88 (m, 4H), 6.78 (br s, 4H), 6.63 (m, 8H), 6.47 (m, 4H), 6.33 (m, 4H), 5.62 (br, 4H), 1.74–0.95 (m, 144H). ESI-MS: *m*/*z* 3901 (M$^+$). Anal. Calcd for C$_{176}$H$_{208}$O$_{16}$Ru$_8$S$_{16}$: C 54.19, H 5.37; found: C 54.30, H 5.37.

Wheel-to-rhomboid isomerization of (○)-[Ru(S-*p*-^{t}BuC$_6$H$_4$)$_2$(CO)$_2$]$_8$. A mixture of (○)-[Ru(S-*p*-^{t}BuC$_6$H$_4$)$_2$(CO)$_2$]$_8$ (75 mg, 0.02 mmol) and 4-*tert*-butyl-benzenethiol (1.0 mL) was heated at 160 °C under nitrogen for 4 h. After the mixture was cooled to room temperature, *n*-pentane (5 mL) was added. The yellow precipitate in the mixture

was collected by filtration, washed with *n*-pentane, and dried. Yield: ~67%. ^{1}H NMR analysis revealed that the product is mainly (◇)-[Ru(S-*p*-^{t}BuC$_6$H$_4$)$_2$(CO)$_2$]$_8$, together with minor amount of (○)-[Ru(S-*p*-^{t}BuC$_6$H$_4$)$_2$(CO)$_2$]$_8$ (ratio of the (◇)-isomer to (○)-isomer: 4:1).

Typical procedure for aziridination of alkenes catalysed by (○)-[Ru(S-*p*-^{i}PrC$_6$H$_4$)$_2$(CO)$_2$]$_6$ and (○)-{Cu[Ru(S-*p*-^{i}PrC$_6$H$_4$)$_2$(CO)$_2$]$_6$}PF$_6$. A mixture of PhI=NTs (74.6 mg, 0.2 mmol) and (○)-[Cu{Ru(S-*p*-^{i}PrC$_6$H$_4$)$_2$(CO)$_2$}$_6$]PF$_6$ (5.8 mg, 1 mol%) was dissolved in anhydrous MeCN (2 mL) followed by addition of alkene (0.6 mmol). The mixture was heated at 80 ℃ under argon for 4 h. The colour of solution changed from pale yellow to dark brown. After the reaction mixture cooled to room temperature, the solution was immediately allowed to pass through a celite column. The celite column was then washed by ethyl acetate three times to extract all the organic components. The combined filtrate was evaporated to dryness in vacuo; the residue was analysed by ^{1}H NMR, using 1,1-diphenylethene as internal standard, to determine the yield of the aziridine product. The aziridine products involved in this work were identified by comparison with their spectral data reported in the literature.[2]

X-ray crystal structure determinations. The crystals, which were obtained by recrystallization from chloroform/pentane, were sealed inside the glass capillaries for data collection at low temperature (173 and 100 K for the Os and Ru complexes, respectively) on a BRUKER X8 PROTEUM diffractometer equipped with microfocus MicroStar rotating anode Cu X-ray generator. Upon removal from mother liquid, the crystals were found to lose solvent rapidly. For the silver(I) complex (◇)-{Ag[Ru(S-*p*-^{t}BuC$_6$H$_4$)$_2$(CO)$_2$]$_8$}$^+$, its crystal became darkened in colour after overnight X-ray exposure. The integrated intensities of the dataset were manually scaled and corrected for sample decomposition due to radiation damage using a linear equation for B value refinement implemented in SADABS program. The diffracting power of the crystals was only reasonably satisfactory, as evidenced by the data completeness (90% and 92.4% for the Os and Ru complexes, respectively); replicate data collection using our high-power X-ray diffractometer did not significantly improve the data completeness. The structures were solved by the direct method. Structure solution and refinement were performed using SHELX-97 suite program.[3] There was very large void volume in the crystal lattice of (◇)-{Ag[Ru(S-*p*-^{t}BuC$_6$H$_4$)$_2$(CO)$_2$]$_8$}$^+$; attempts to locate sensible peaks for the counter ion $CF_3SO_3^-$ were not successful. The residual peaks from the void space were likely recognized as atoms of the solvent molecules ($CHCl_3$) and subsequent refinement of their thermal parameters with bond/angle restraints was also achieved.

Without locating the counterion $CF_3SO_3^-$ for the Ru crystal, selected peaks with significant electron density (4–5 e $Å^{-3}$) were modelled as chloride ions that were statistically disordered with partial occupancies in the lattice, that in theory were equal to that (50%) of the bound metal cation (Ag^+). The Cl···Cl and Cl···H distances of the assigned chloride ion in the complex were approximately 3.11-3.50 Å and 2.76-3.10 Å, that were chemically consistent with the literature values. Due to insufficient data at high resolution limit, the current model containing solvent molecules and severely disordered counterion was refined to give a relatively high *R*-factor of ~14%. The position and thermal parameters of all non-hydrogen atoms in the Ru crystal were anisotropically refined as usual.

References

1 S. L.-F. Chan, L. Shek, J.-S. Huang, S. S.-Y. Chui, R. W.-Y. Sun and C.-M. Che, *Angew. Chem., Int. Ed.*, 2012, **51**, 2614.

2 (*a*) H. Han, I. Bae, E. J. Yoo, J. Lee, Y. Do and S. Chang, *Org. Lett.* **2004**, *6*, 4109; (*b*) G.-Y. Gao, J. D. Harden and X. P. Zhang, *Org. Lett.*, 2005, **7**, 3191; (*c*) Z. Li, X. Ding and C. He, *J. Org. Chem.*, 2006, **71**, 5876.

3 G. M. Sheldrick, *Acta Crystallogr*., 2008, **A64**, 112.

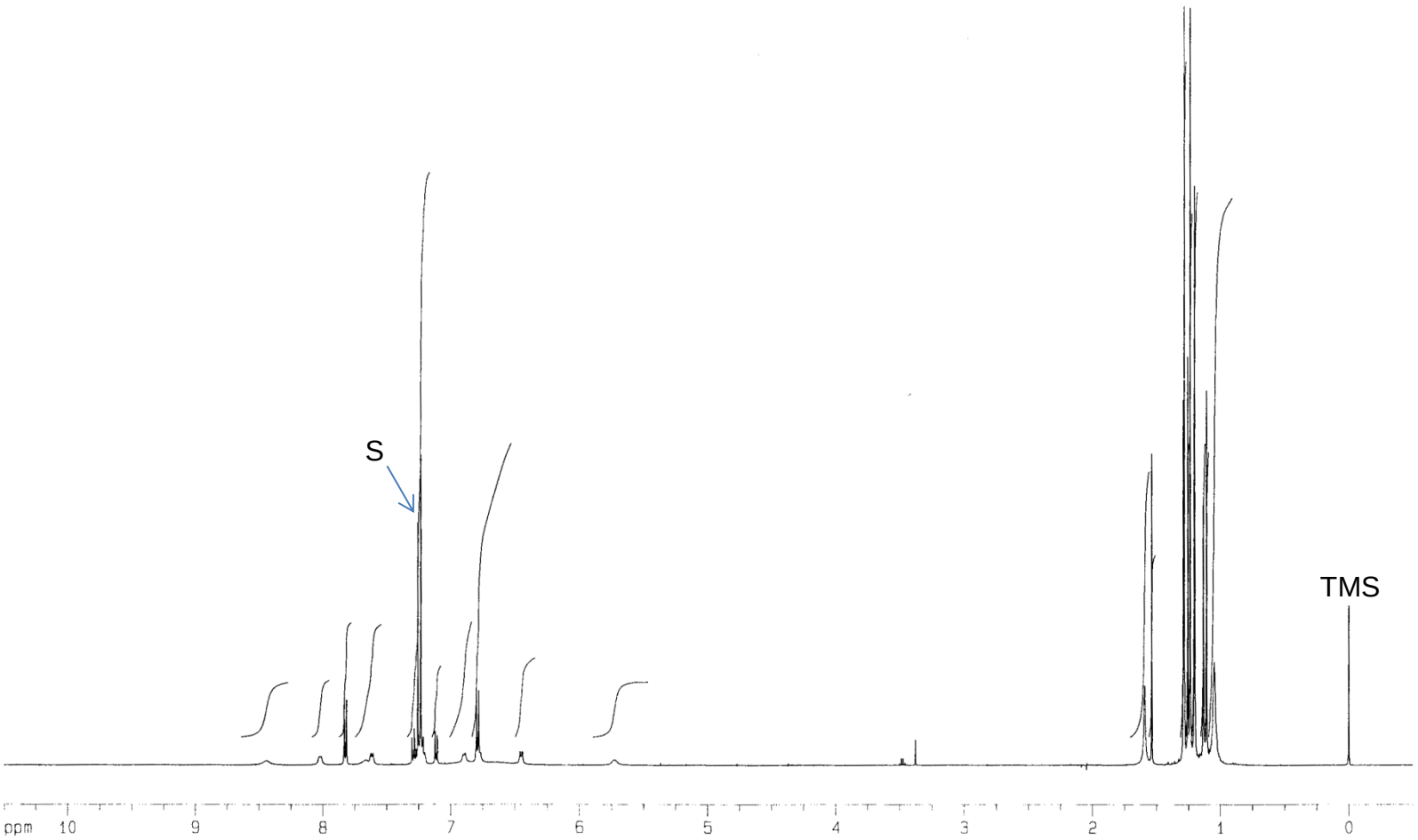

Fig. S1 ^{1}H NMR spectrum (500 MHz) of a mixture of (○)- and (◇)-[Os(S-*p*-^{t}BuC$_6$H$_4$)$_2$(CO)$_2$]$_8$ in CDCl$_3$ at 298 K.

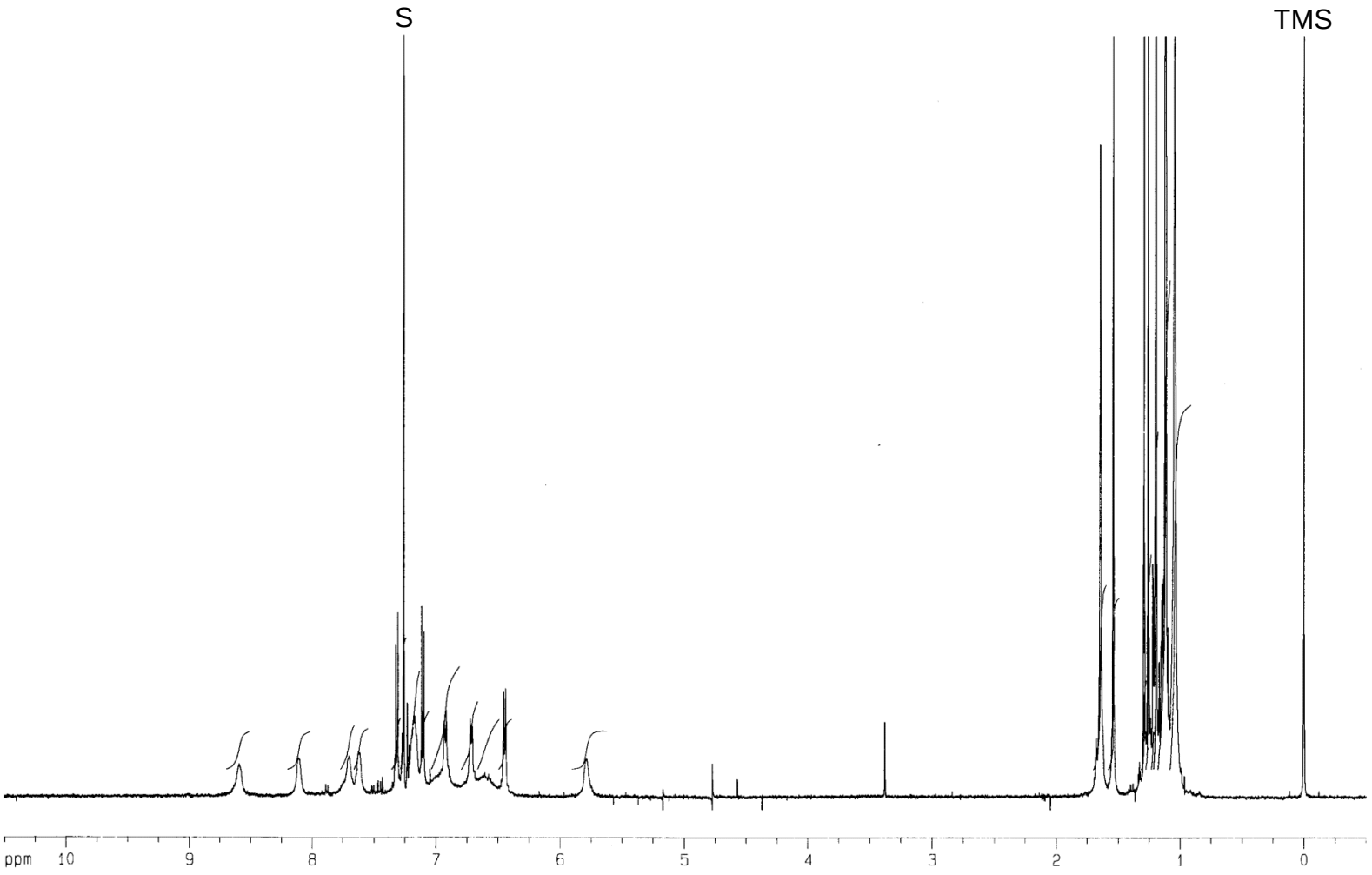

Fig. S2 ^{1}H NMR spectrum (500 MHz) of (◇)-[Ru(S-*p*-^{t}BuC$_6$H$_4$)$_2$(CO)$_2$]$_8$ in CDCl$_3$ at 298 K.

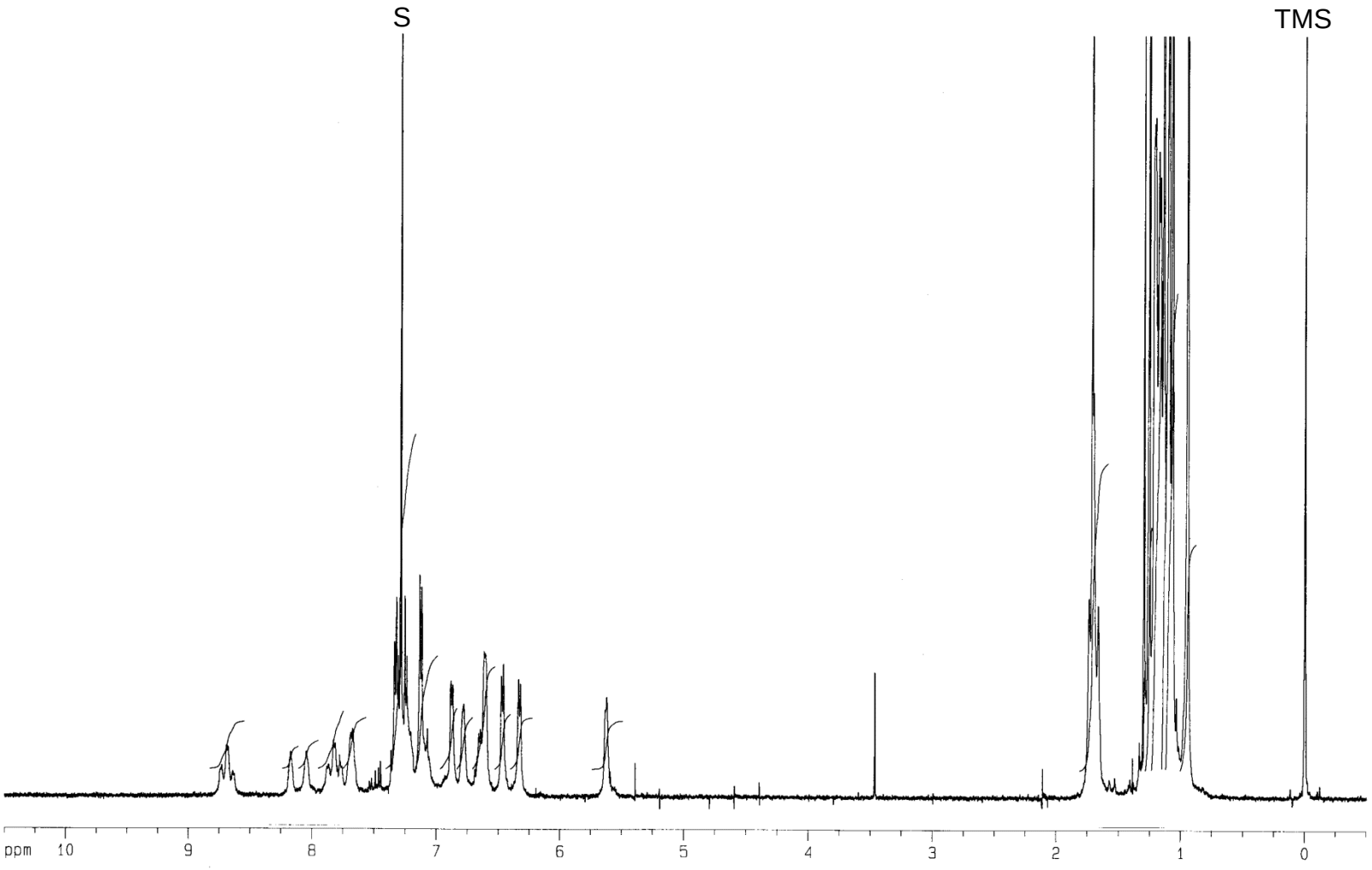

Fig. S3 ^{1}H NMR spectrum (500 MHz) of (◇)-[Ru(S-*p*-^{t}BuC$_6$H$_4$)$_2$(CO)$_2$]$_8$ in $CDCl_3$ at 253 K.

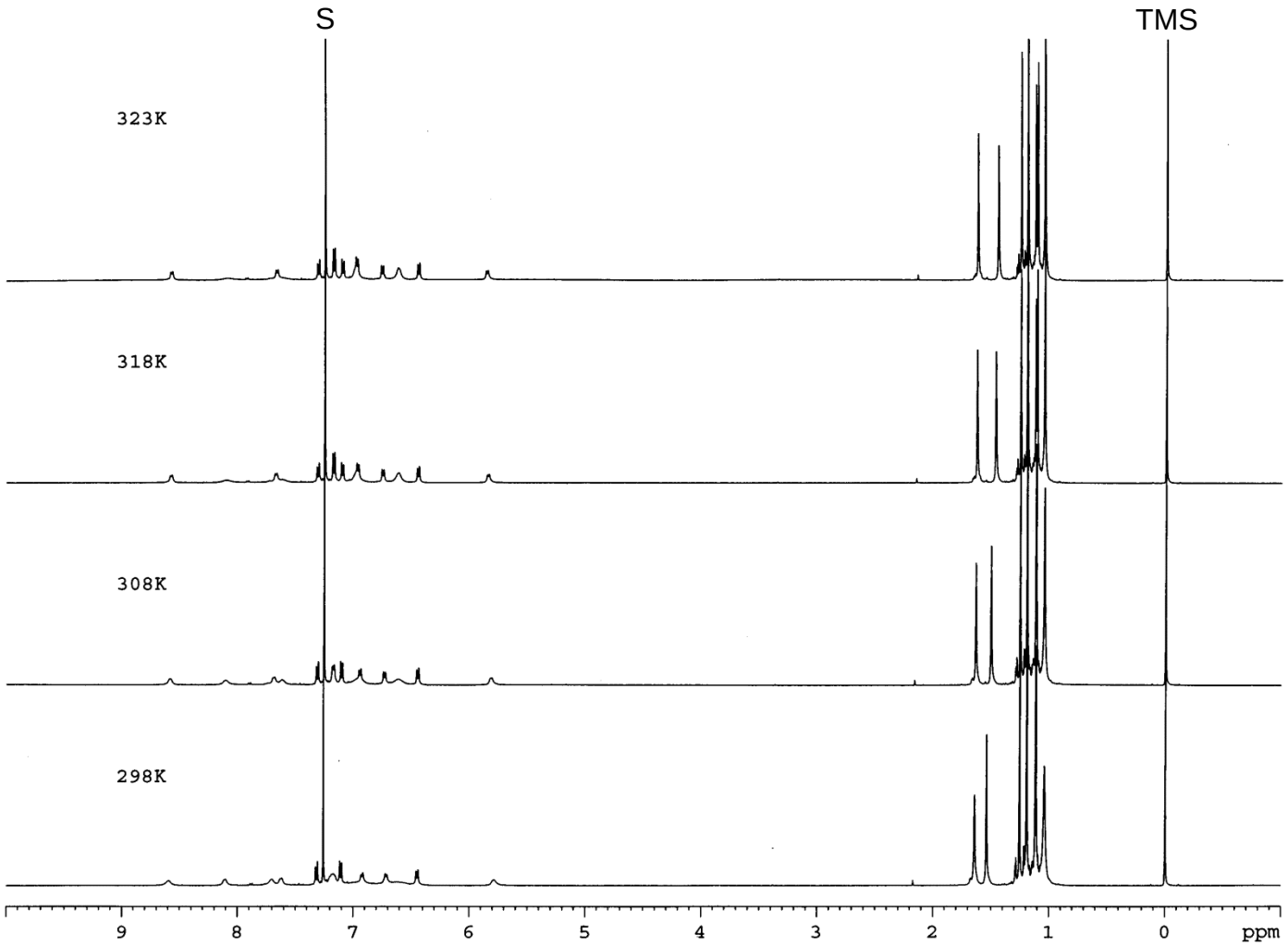

Fig. S4 ^{1}H NMR spectrum (500 MHz) of (◇)-[Ru(S-*p*-^{t}BuC$_6$H$_4$)$_2$(CO)$_2$]$_8$ in CDCl$_3$ at 298–323 K.

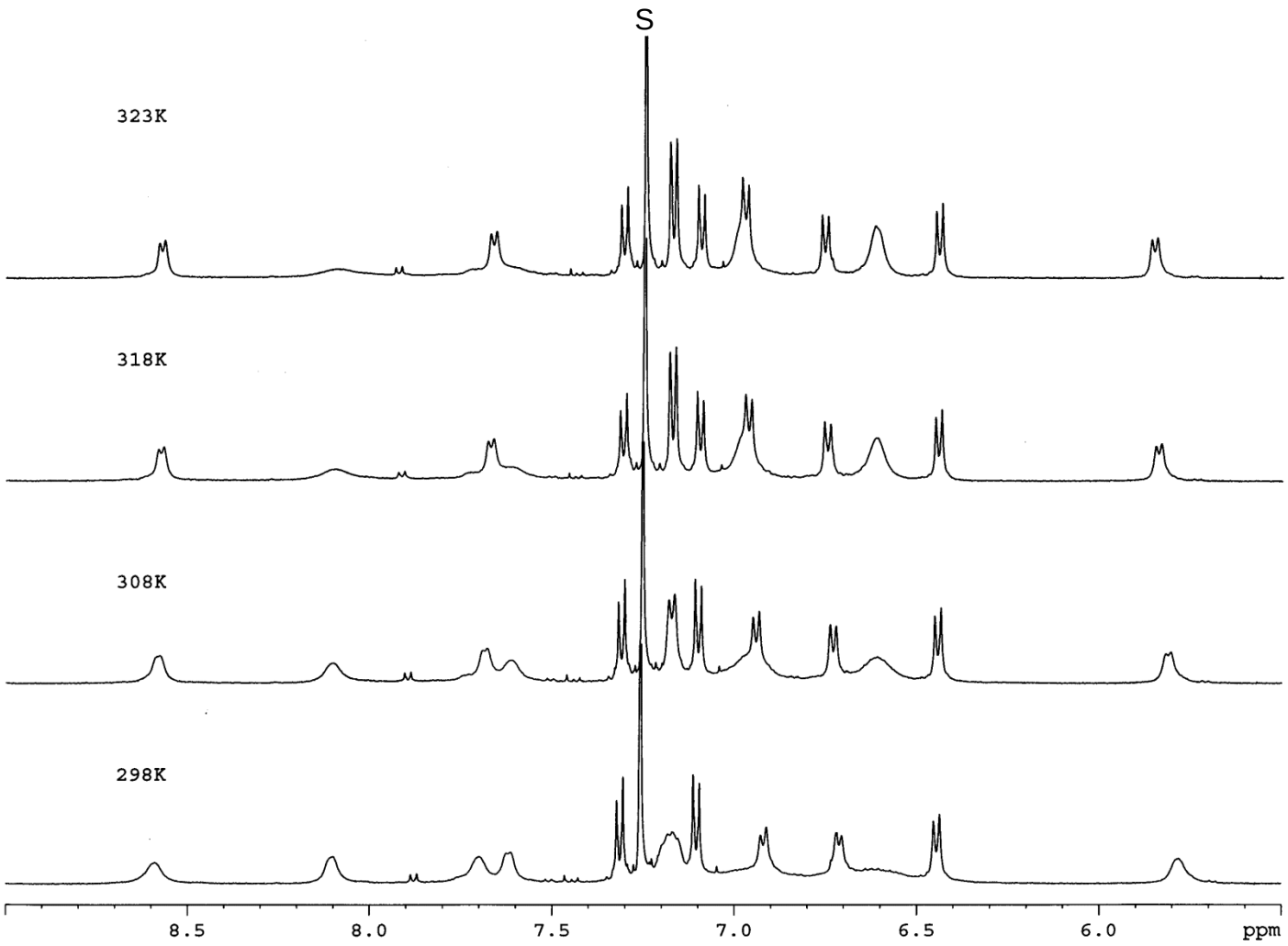

Fig. S5 ^{1}H NMR spectrum (500 MHz, aromatic region) of (◇)-[Ru(S-*p*-^{t}BuC$_6$H$_4$)$_2$(CO)$_2$]$_8$ in CDCl$_3$ at 298–323 K.

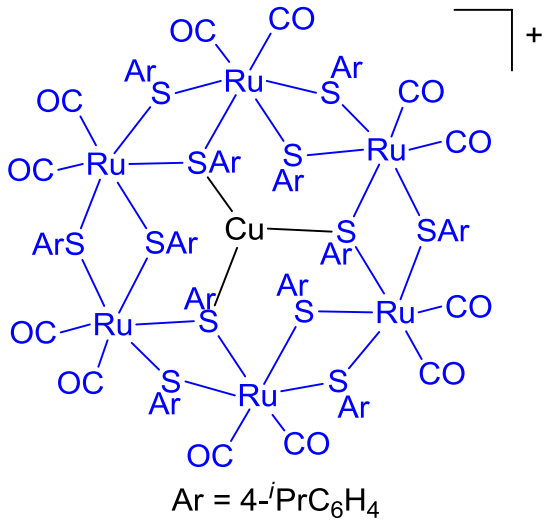

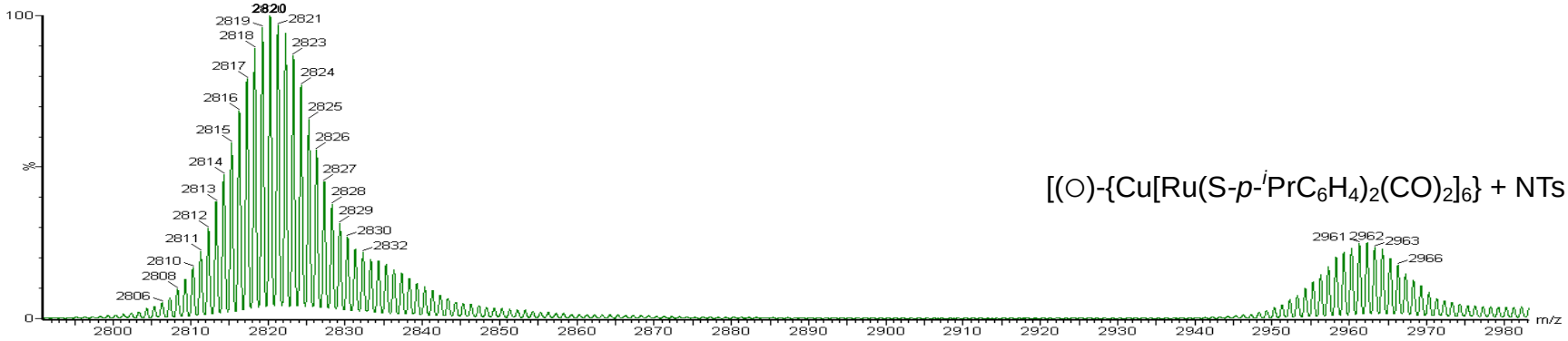

[(○)-{Cu[Ru(S-*p*-^{i}PrC$_6$H$_4$)$_2$(CO)$_2$]$_6$} + NTs – CO]$^{+}$

Fig. S6 ESI-MS measurement of a reaction mixture of (○)-{Cu[Ru(S-*p*-^{i}PrC$_6$H$_4$)$_2$(CO)$_2$]$_6$}$^{+}$ with PhI=NTs (4 equiv) in CH_2Cl_2 after 3 min.

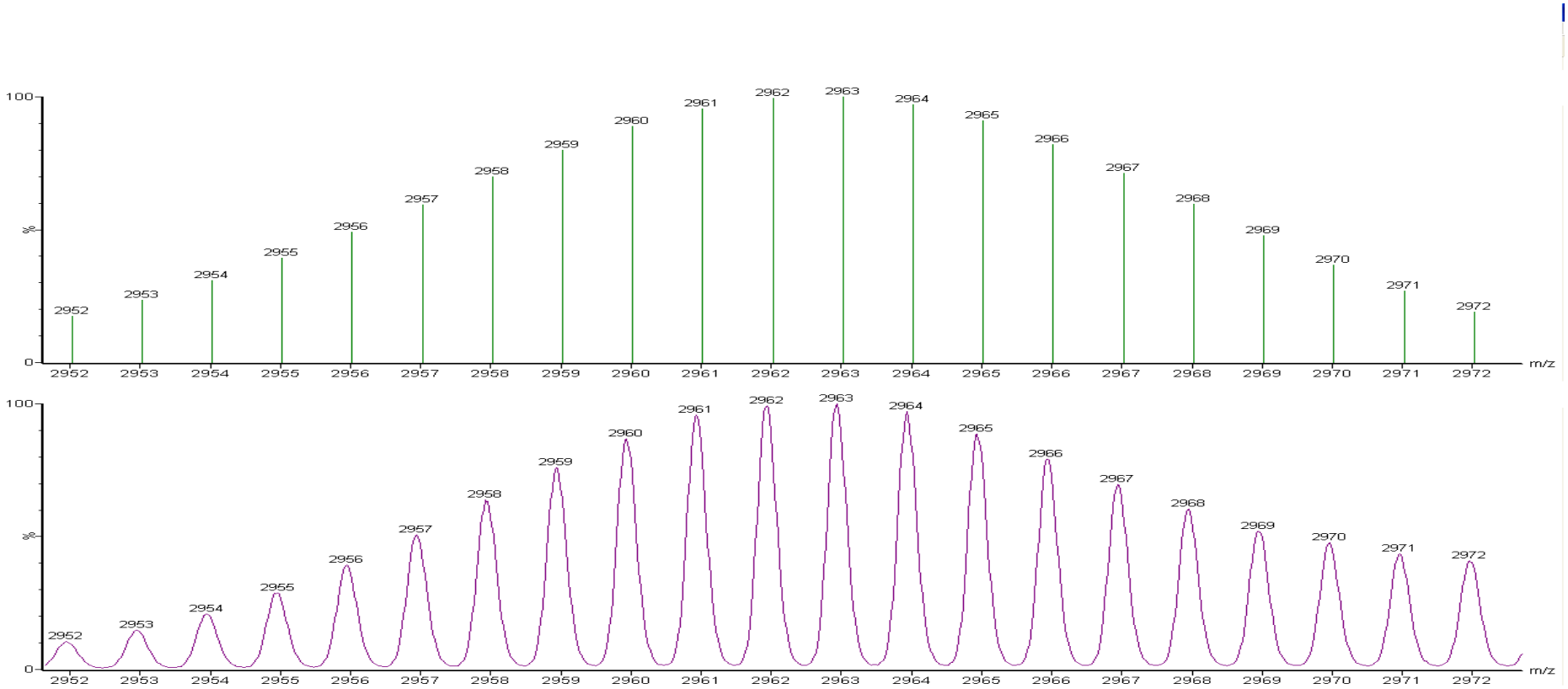

Fig. S7 Lower: Zoom-scan at *m*/*z* 2962 for ESI-MS measurement of a reaction mixture of (○)-{Cu[Ru(S-*p*-^{i}PrC$_6$H$_4$)$_2$(CO)$_2$]$_6$}$^+$ with PhI=NTs (4 equiv) in CH_2Cl_2 after 3 min. Upper: Simulated isotope pattern for [(○)-{Cu[Ru(S-*p*-^{i}PrC$_6$H$_4$)$_2$(CO)$_2$]$_6$} + NTs – CO]$^+$.

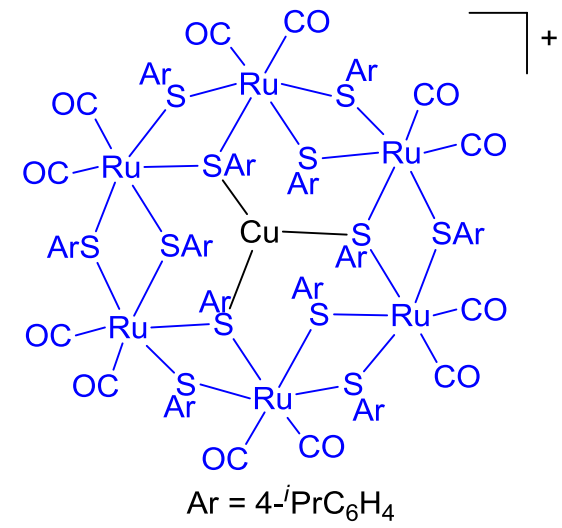

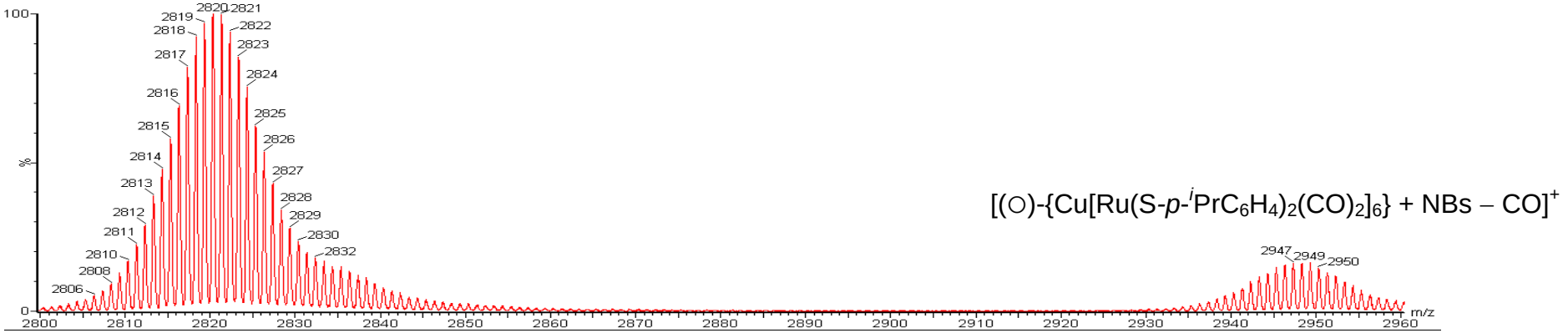

Fig. S8 ESI-MS measurement of a reaction mixture of (○)-{Cu[Ru(S-*p*-^{i}PrC$_6$H$_4$)$_2$(CO)$_2$]$_6$}$^{+}$ with PhI=NBs (4 equiv) in CH_2Cl_2 after 3 min.

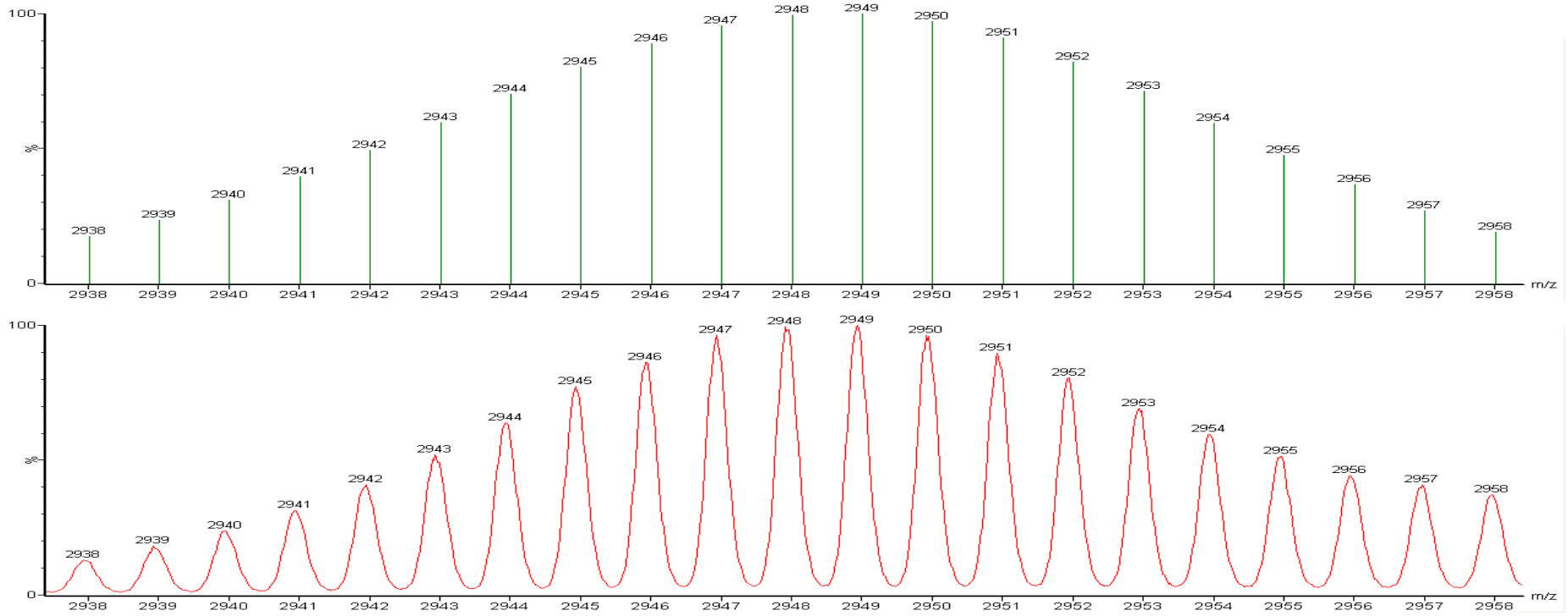

Fig. S9 Lower: Zoom-scan at *m*/*z* 2948 for ESI-MS measurement of a reaction mixture of (○)-{Cu[Ru(S-*p*-^{i}PrC$_6$H$_4$)$_2$(CO)$_2$]$_6$}$^+$ with PhI=NBs (4 equiv) in CH_2Cl_2 after 3 min. Upper: Simulated isotope pattern for [(○)-{Cu[Ru(S-*p*-^{i}PrC$_6$H$_4$)$_2$(CO)$_2$]$_6$} + NBs – CO]$^+$.

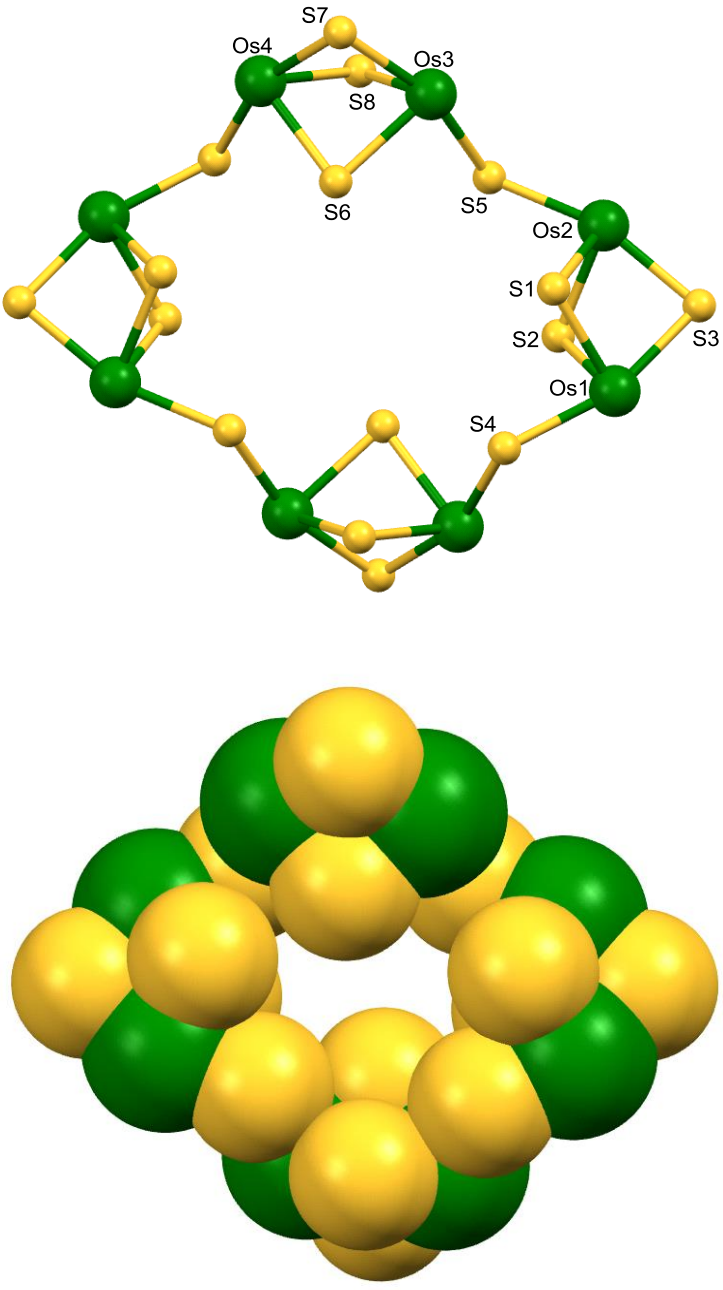

Fig. S10 Metallacycle core in crystal structure of (◇)-[Os(S-*p*-^{t}BuC$_6$H$_4$)$_2$(CO)$_2$]$_8$. Upper: Ball and stick representation. Lower: Space-filling representation.

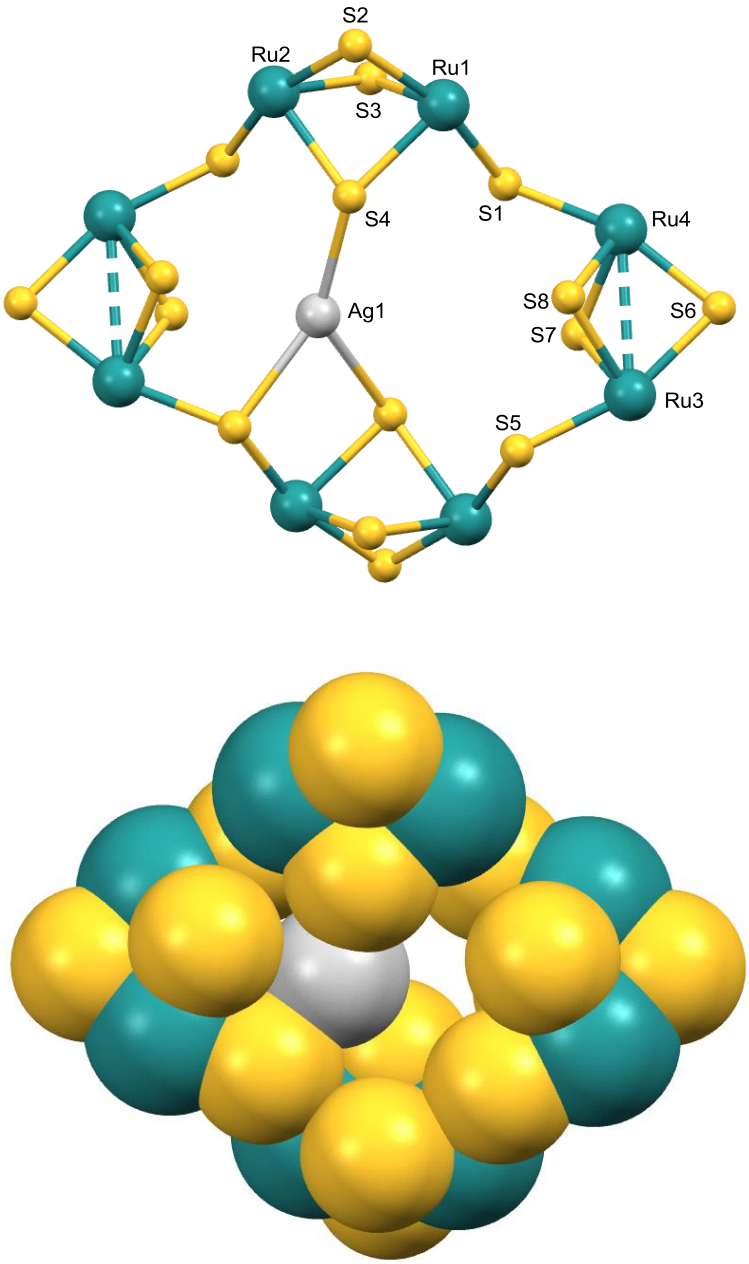

Fig. S11 Metallacycle core and the bound Ag(I) in crystal structure of (◇)-{Ag[Ru(S-*p*-^{t}BuC$_6$H$_4$)$_2$(CO)$_2$]$_8$}$^{+}$. Upper: Ball and stick representation. Lower: Space-filling representation.

Table S1 Selected bond distances and angles for (◇)-[Os(S-*p*-^{t}BuC$_6$H$_4$)$_2$(CO)$_2$]$_8$.

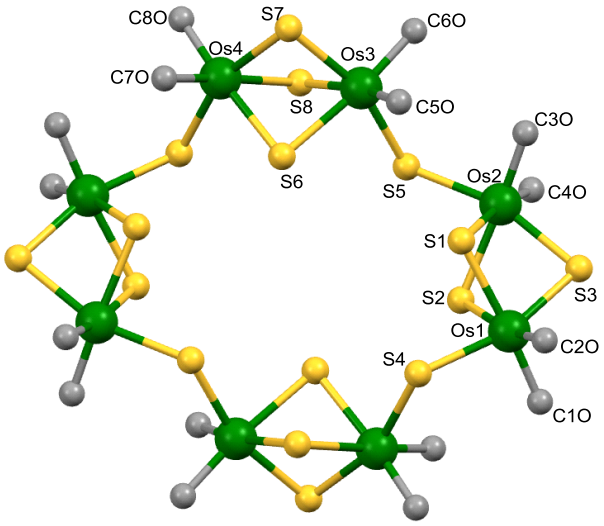

Bond distances (Å)			
Os1–C1O	1.879(7)	Os1–C2O	1.895(8)
Os2–C3O	1.860(7)	Os2–C4O	1.898(8)
Os3–C5O	1.910(8)	Os3–C6O	1.874(8)
Os4–C7O	1.880(8)	Os4–C8O	1.873(8)
Os1–S1	2.4829(17)	Os1–S2	2.4667(17)
Os1–S3	2.4180(18)	Os1–S4	2.4195(17)
Os2–S1	2.4512(19)	Os2–S2	2.5019(17)
Os2–S3	2.4229(17)	Os2–S5	2.4256(16)
Os3–S5	2.4229(17)	Os3–S6	2.4977(17)
Os3–S7	2.4183(19)	Os3–S8	2.4568(19)
Os4–S6	2.4889(17)	Os4–S7	2.4188(19)
Os4–S8	2.4512(19)	Os4–S4′	2.4276(18)

Bond angles (°)			
Os2-S1-Os1	84.78(6)	Os1-S2-Os2	84.05(5)
Os1-S3-Os2	86.81(6)	Os3-S5-Os2	125.17(7)
Os4-S6-Os3	83.96(5)	Os3-S7-Os4	87.19(6)
Os4-S8-Os3	85.62(6)	Os1- S4-Os4′	121.57(8)
C1O-Os1-S1	175.4(2)	C2O-Os1-S2	168.9(2)
C4O-Os2-S1	169.8(2)	C3O-Os2-S2	174.2(2)
C6O-Os3-S6	173.3(2)	C8O-Os4-S6	171.6(3)
C5O-Os3-S8	169.7(2)	C7O-Os4 S8	174.2(2)

Table S2 Selected bond distances and angles for (◇)-{Ag[Ru(S-*p*-^{t}BuC$_6$H$_4$)$_2$(CO)$_2$]$_8$}$^{+}$.

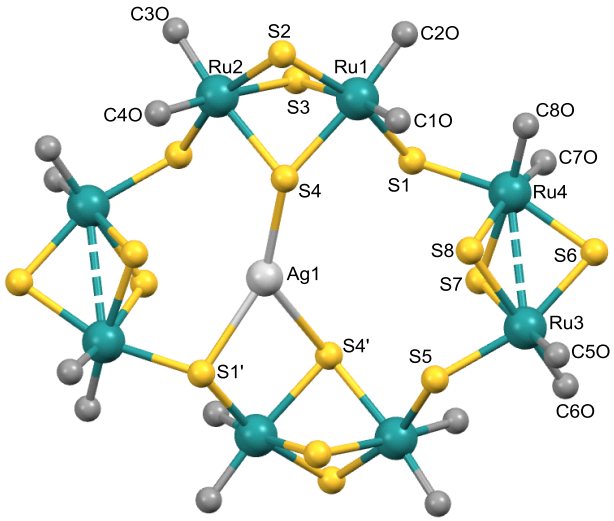

Bond distances (Å)			
Ru1–C1O	1.921(12)	Ru1–C2O	1.859(15)
Ru2–C3O	1.871(13)	Ru2–C4O	1.915(13)
Ru3–C5O	1.939(15)	Ru3–C6O	1.886(13)
Ru4–C7O	1.875(15)	Ru4–C8O	1.877(14)
Ru1–S1	2.411(2)	Ru1–S2	2.425(3)
Ru1–S3	2.419(3)	Ru1–S4	2.506(3)
Ru2–S2	2.428(3)	Ru2–S3	2.436(3)
Ru2–S4	2.509(3)	Ru2–S5′	2.405(3)
Ru3–S5	2.409(3)	Ru3–S6	2.409(3)
Ru3–S7	2.433(3)	Ru3–S8	2.471(3)
Ru4–S1	2.419(3)	Ru4–S6	2.404(3)
Ru4–S7	2.461(3)	Ru4–S48	2.433(3)
Ag1–S1′	2.656(3)	Ag1–S4	2.594(3)
Ag1–S4′	2.792(3)	Ru3···Ru4	3.218(3)

Bond angles (°)			
Ru2-S2-Ru1	84.49(10)	Ru1-S3-Ru2	84.44(9)
Ru1-S4-Ru2	81.16(8)	Ru1-S1-Ru4	124.36(12)
Ru4-S6-Ru3	83.92(10)	Ru3-S7-Ru4	82.22(10)
Ru4-S8-Ru3	82.02(8)	Ru3- S5-Ru2′	124.59(11)
C1O-Ru1-S3	171.7(4)	C2O-Ru1-S4	173.3(5)
C4O-Ru2-S3	176.3(4)	C3O-Ru2-S4	171.6(4)
C6O-Ru3-S8	177.0(5)	C8O-Ru4-S7	174.4(4)
C5O-Ru3-S7	170.4(4)	C7O-Ru4-S8	168.5(5)
S4-Ag1-S1	145.15(10)	S4-Ag1-S4′	135.25(8)
S1′-Ag1-S4′	77.16(9)		